Biodegradation of Functionalized Nanocellulose

Benjamin P. Frank[1], Casey Smith[1], Emily R. Caudill[2], Ronald S. Lankone[1], Katrina Carlin[1], Sarah J. Benware,[2] Joel A. Pedersen[2], D. Howard Fairbrother[1]

[1]Department of Chemistry, Johns Hopkins University, 3400 N Charles Street, Baltimore, MD 21218, United States

[2]Department of Chemistry, University of Wisconsin-Madison, 1101 University Avenue, Madison, Wisconsin 53706, United States

Supporting Information

23 Pages, 15 Figure, 9 Tables

Materials Characterization

ATR-FTIR. Attenuated total reflectance Fourier-transform infrared spectroscopy data of CNF powders were obtained with a Nicolet iS5 spectrometer and an iD5 ATR attachment with a diamond stage using a scan range from 4000 cm^{-1} to 525 cm^{-1} at 0.964 cm^{-1} resolution with 32 scans collected and averaged per measurement.

CHN Elemental Analysis. CHN elemental analyses were performed to determine $DS_{overall}$ for functionalized CNFs. Tests were performed on an Exeter Analytical CE440 CHN Analyzer at the Microanalysis Laboratory at University of Illinois at Urbana-Champaign. Dried samples (2.0 – 3.0 mg) were weighed into consumable tin capsules, placed in an autosampler wheel, and purged with helium. The capsule was driven into a high temperature (1000 °C) furnace and combusted in pure oxygen under static conditions. The resulting combustion products containing carbon dioxide (CO_2), water (H_2O), nitrogen (N_2) and oxides of nitrogen (NO_x) were passed over copper to scrub excess oxygen and reduce oxides of nitrogen to elemental nitrogen. After scrubbing, the gases entered a mixing volume chamber to ensure a homogeneous mixture at constant temperature and pressure. The mixture then passed through a series of high-precision thermal conductivity detectors to determine the CHN content in two replicates of each sample.

Solid-State NMR. Solid-state NMR spectra were collected at the University of Wisconsin – Madison on a Bruker Avance III 500 MHz spectrometer equipped with a 4 mm cross-polarization magic angle spinning (CP-MAS) probe. Cross polarization experiments were performed, wherein the peak intensity and area depend on both the abundance of the observed nuclei and the number of protons on nearby probed carbon nuclei (within 3-4 Å). The ^{13}C spectra were externally referenced using adamantine (upfield peak was set to 38.5 ppm). Spectra were acquired at 298 K at a rotational speed of 12 kHz. Other experimental acquisition details are previously reported.[1]

All spectra were processed in MestReNova, including baseline correction and manual phase correction. Peaks corresponding to amorphous or crystalline forms of CNF were assigned based on known chemical shifts,[2] and the proportion of crystalline and amorphous character was determined by averaging these respective peak areas.

Variable contact time (VCT) cross polarization–magic-angle spinning (CP-MAS) experiments were conducted to estimate $DS_{overall}$ from ^{13}C NMR data for two samples: phenyl ester CNF and DA-CNF-2. The molecular motion of the aromatic ring in the phenyl ester was expected to exhibit slower molecular motion than the long aliphatic chain in the dodecyl ester and lead to a shorter relaxation time constant of protons in the rotating frame ($T_{1\rho H}$). Phenyl ester CNF and DA-CNF-2 spectra were recorded with spinning at 12 and 11 kHz, respectively. A 2.5 µs 90° proton pulse was followed by a variable contact time of 700 to 7500 µs, high power proton decoupling during acquisition, and a relaxation delay of 6 s. We determined $T_{1\rho H}$ via CP experiments with varied ^{1}H spin-lock duration from 1,000 to 15,000 µs before application of the ^{13}C spin lock and a contact time of 2000 µs. For the $T_{1\rho H}$ experiments, phenyl ester CNF was spun at 9.5 kHz and DA-CNF-2 was spun at 11 kHz. For all spectra, 1024 scans were acquired with a sweep width of 497 ppm. Each peak in the spectra was approximated by a Gaussian function curve fitting analysis.

Signal intensity (M_1) was plotted as a function of contact time (t) for each ^{13}C species and the data were fit to the equation

$$M_1 = \frac{M_0 \frac{\gamma_H}{\gamma_C}}{1 - \frac{T_{CH}}{T_{1\rho H}}} [e^{\left(-\frac{t}{T_{1\rho H}}\right)} - e^{\left(-\frac{t}{T_{CH}}\right)}] \tag{S1}$$

where γ_H and γ_C are the gyromagnetic ratios of ^{1}H and ^{13}C, T_{CH} is the cross-polarization time constant, and M_0 is the magnitude of the equilibrium magnetization which is directly proportional

to the concentration of a given ^{13}C species in a sample.[3] To fit the data from the set of standard CP experiments, calculated $T_{1\rho H}$ values were constrained while M_0 and T_{CH} values were varied through an iterative non-linear least squares fitting. The resulting curve fits are shown in Figure S11. We calculated $T_{1\rho H}$ from the negative inverse of the slope of a linear fit of ln(signal intensity) as a function of duration of ^1H spin-lock before contact time. For both samples, there appeared to be multiple $T_{1\rho H}$ in the rotating frame affecting the signal intensities of the substituents, and a global $T_{1\rho H}$ affecting cellulose carbon signal intensity. Nonetheless, for phenyl ester CNF, the $T_{1\rho H}$ calculated for aromatic carbons (3700 ± 448.5 μs) allowed a good fit of the VCT data (Fig. S11). For DA-CNF-2, however, the $T_{1\rho H}$ calculated for the entire range of ^1H spin lock duration did not represent the observed decay in intensity in the VCT data. For this reason, the initial linear region (1000-7000 μs) of the data was used to calculate a $T_{1\rho H}$ of 18000 ± 1000 μs which fit the VCT data well (Figure S11).

We calculated $DS_{overall}$ for phenyl ester CNF according to the equation $DS = 1.2 \times M_A/M_C$, where M_A is the M_0 of aromatic carbons, M_C is the M_0 for cellulose carbons, and the factor of 1.2 normalizes the value to the number of carbons contributing to the intensity of each signal. We calculated $DS_{overall}$ for DA-CNF-2 according to the equation $DS = 6 \times M_{Me}/M_C$, where M_{Me} is the M_0 for the methyl carbon on the dodecyl ester substituent, and 6 is a normalization factor. The standard error in the M_0 values were propagated through the $DS_{overall}$ calculations (Table S8).

The $DS_{overall}$ for phenyl ester CNF was estimated to be 0.09 from the VCT experiments and was determined to be 0.14 by elemental analysis (Table S8). For the DA-CNF-2 sample, $DS_{overall}$ estimated from VCT experiments was 0.19 while that obtained from elemental analysis was 0.45. The $DS_{overall}$ from VCT experiments is calculated from the normalized ratio of intensities of carbon on the substituent to the sum of intensities of cellulose carbons. We note that multiple $T_{1\rho H}$

behavior was observed for signals for the substituents on phenyl ester CNF and DA-CNF-2, which could be a source of error responsible for the disagreement between $DS_{overall}$ from VCT and elemental analysis.

X-ray Photoelectron Spectroscopy. X-ray photoelectron spectra of CNF powders were obtained to determine $DS_{surface}$ using a PHI 5600 XPS equipped with a Mg Kα flood source (1253.6 eV) and a hemispherical energy analyzer. High resolution multiplex scans were collected at ultra-high vacuum (8×10^{-8} torr) using a source power of 300 W, pass energy 23.5 eV, 10 sweeps per spectrum, and 0.025 eV/step. Survey scans were collected from 1200 eV to 0 eV at the same ultra-high vacuum and power but with a pass energy of 187.85 eV, two sweeps per spectrum, and 1.6 eV/step. Spectra were analyzed using CASA XPS software.

Biomethane Potential Tests

Our assertion that the biogas measured as a comparison of biodegradation is supported by the comparatively low mass of carbon in the BMP media. The BMP media recipe shown in Table S3 is primarily inorganic, with trace amounts of organic nutrients. Each sample was digested in 100 mL of this media. By using the wt% of C in each organic component of this media and diluting each stock to the final concentration in 100 mL of media (i.e., volume used to incubate samples), only 0.075 mg C is contributed by these nutrients. This is compared to ~42 mg of C added in a 100 mg sample of unmodified CNF. Importantly, these residual organics only contribute minimal biogas production as evidenced by our blank controls (media including sludge in absence of CNF sample) which produced ~10 mL on average over 75 days compared to > 100 mL for CNF. The biogas evolved from the blanks primarily comes from the small organic content of the digested sludge. The overall carbon contribution from this component is small, as the % total solids (%TS) of digested sludge is under 10%, and often around 5-6%, otherwise the anaerobic digester is not

operating as intended, and samples would not have been available.[4-6] For our tests, roughly 55% of the mass of these solids are considered "volatile" (data not shown). Included in these volatile solids (VS) are the biodegradable components of sludge, while the residual solids are typically inorganic or highly recalcitrant to biodegradation (i.e., they persist after heating at 550 °C for 2 hr in standard sludge characterization tests). Because the volatile solids fraction is only partially biodegradable (~60% for undigested sludge, less for digested sludge as was used here), each sample has only a small amount of theoretically biodegradable material contributed by the sludge, and only a portion of this material will consist of C.[7] The minimal contribution of biogas by the blank controls suggests that most of the biogas produced in these BMP tests was evolved by the cellulosic samples being investigated.

Aerobic Biodegradation Tests.

Recovery of powdered samples was facilitated by the initial centrifugation step before the addition of primary effluent. By pelletizing each powder into the bottom of the vials prior to addition of the primary effluent, the solids were prevented from dispersing into the aqueous media. This permitted us to pipette off the supernatant media at the conclusion of the biodegradation experiment without disturbing the pelletized portion of the sample. Each powder was then recovered, washed with ethanol and MilliQ water, and dried before massing. While we cannot exclude a small contribution of residual biomass to the final mass of our samples, such a contribution can be safely neglected in comparing the relative biodegradability of the samples due to this washing step.

Tables

Table S1. Elemental composition and calculated $DS_{overall}$ for cellulose nanofibrils (CNFs) functionalized with ether and ester groups.

Sample	%C	%H	%N	%O	$DS_{overall}$
Cellulose Nanofibrils	41.53	6.07	0	52.4	0
Hexyl Ester CNF	42.80	6.30	0	50.90	0.09
Phenyl Ester CNF	44.75	5.86	0	49.39	0.14
Dodecyl Ether CNF	45.41	6.85	0.11	47.63	0.11
Hexyl Ether CNF	42.18	5.84	0.05	51.93	0.05
GP-HC-CNF-1	-	-	-	-	-
GP-HC-CNF-2	-	-	-	-	-
GP-HC-CNF-3	-	-	-	-	-
GP-HC-CNF-4	43.60	5.96	0.13	50.31	0.14
GP-LC-CNF-1	-	-	-	-	-
GP-LC-CNF-2	-	-	-	-	-
GP-LC-CNF-3	-	-	-	-	-
GP-LC-CNF-4	41.75	5.93	0.14	52.18	0.013
LC-CNF-1	58.45	9.31	0.55	31.69	0.80
LC-CNF-2	58.69	9.18	0.47	31.66	0.82
LC-CNF-3	55.26	8.51	0.36	35.87	0.56
LC-CNF-4	61.96	9.66	0.70	27.68	1.16
DA-CNF-1	42.56	6.27	0.08	51.09	0.035
DA-CNF-2	53.04	8.15	0.10	38.71	0.45
DA-CNF-3	49.47	7.42	0.08	43.03	0.28
DA-CNF-4	47.33	6.99	0.95	44.73	0.20

Table S2. X-ray photoelectron spectra %C–C component values and calculated $DS_{surface}$ for cellulose nanofibrils functionalized with different ether and ester groups.*

Sample	%C-C	$DS_{surface}$
Cellulose Nanofibrils	14.5	0
Hexyl Ester CNF	17.1	0.03
Phenyl Ester CNF	25.1	0.17
Dodecyl Ether CNF	30.2	0.16
Hexyl Ether CNF	25.2	0.25
GP-HC-CNF-1	53.1	1.19
GP-HC-CNF-2	58.7	1.54
GP-HC-CNF-3	63.2	1.89
GP-HC-CNF-4	68.4	2.43
GP-LC-CNF-1	20.7	0.07
GP-LC-CNF-2	30.8	0.17
GP-LC-CNF-3	35.8	0.23
GP-LC-CNF-4	42.7	0.33
LC-CNF-1	56.3	0.63
LC-CNF-2	57.8	0.67
LC-CNF-3	68.7	1.12
LC-CNF-4	82.3	2.46
DA-CNF-1	15.1	0.014
DA-CNF-2	24.2	0.097
DA-CNF-3	28.8	0.15
DA-CNF-4	47.9	0.43

* %C-C values calculated using CASAXPS software.
Cellulose Nanofibrils (CNF) are denoted.

Table S3. Biomethane potential (BMP) test stock solutions S1-S7. BMP media consists of 0.9 mL S2, 2.7 mL S3, 13.5 mL S4, 0.9 mL S5, 0.9 mL S6, and 9 mL S7 per liter of ultrapure water and 10% digested wastewater sludge.

Solution	Compound	Concentration, g/L
S1	Sample	<2 g/L degradable COD in assay liquid (estimated)
S2	Resazurin (oxidation-reduction indicator)	1
S3	$(NH_4)_2HPO_4$	26.7
S4	$CaCl_2 \cdot 2H_2O$	16.7
	NH_4Cl	26.6
	$MgCl_2 \cdot 6H_2O$	120
	KCl	86.7
	$MnCl_2 \cdot 4H_2O$	1.33
	$CoCl_2 \cdot 6H_2O$	2
	H_3BO_3	0.38
	$CuCl_2 \cdot 2H_2O$	0.18
	$Na_2MoO_4 \cdot 2H_2O$	0.17
	$ZnCl_2$	0.14
S5	$FeCl_2 \cdot 4H_2O$	370
S6	$Na_2S \cdot 9H_2O$	500
S7	Biotin	0.002
	Folic acid	0.002
	Pyridoxine hydrochloride	0.01
	Riboflavin	0.005
	Thiamine	0.005
	Nicotinic acid	0.005
	Pantothenic acid	0.005
	B12	0.0001
	p-aminobenzoic acid	0.005
	Thioctic acid	0.005

Table S4. Calculated maximum biogas production from each functionalized cellulose nanofibril (CNF).

Sample	Calculated Total Max Biogas (mL/g)	Empirical Total Biogas (mL/g)
CNF	680	680
PhAA CNF	723	668
Hex Acid CNF	674	694
Na$^+$ TEMPO	699	596
H$^+$ TEMPO	699	606
Ethyl Cellulose	699	18
Hexyl Ether	699	105
Dodecyl Ether	699	70
DA-CNF-1	703	665
DA-CNF-2	883	828
DA-CNF-3	823	580
DA-CNF-4	791	524
LC-CNF-1	966	898
LC-CNF-2	970	687
LC-CNF-3	913	561
LC-CNF-4	1021	374
GP-HC-CNF-1	635	638
GP-HC-CNF-2	637	571
GP-HC-CNF-3	642	423
GP-HC-CNF-4	642	448
GP-LC-CNF-1	699	682
GP-LC-CNF-2	694	630
GP-LC-CNF-3	689	605
GP-LC-CNF-4	689	620

Table S5. Gompertz model statistics and parameters* for functionalized cellulose nanofibrils (CNFs).

Sample	RMSE	NRMSE	R^2	Normalized V_{max}	Normalized K	Normalized I
CNF	0.058	0.250	0.977	1.01	0.078	0.68
LC-CNF-1	0.026	0.080	0.995	0.93	0.036	3.01
LC-CNF-2	0.030	0.086	0.989	0.71	0.031	2.82
LC-CNF-3	0.033	0.181	0.976	0.62	0.017	0.00
LC-CNF-4	0.022	0.151	0.979	0.37	0.019	2.96
DA-CNF-1	0.052	0.138	0.986	0.95	0.037	2.70
DA-CNF-2	0.095	0.289	0.937	0.94	0.020	0.00
DA-CNF-3	0.092	0.312	0.897	0.70	0.012	0.00
DA-CNF-4	0.048	0.251	0.968	0.67	0.0090	0.00
GP-HC-CNF-1	0.024	0.172	0.996	1.01	0.031	5.19
GP-HC-CNF-2	0.022	0.127	0.995	0.90	0.023	3.20
GP-HC-CNF-3	0.022	0.079	0.990	0.66	0.013	0.00
GP-HC-CNF-4	0.025	0.123	0.988	0.70	0.013	0.49
GP-LC-CNF-1	0.045	0.410	0.987	0.98	0.082	1.57
GP-LC-CNF-2	0.043	0.163	0.986	0.91	0.046	2.43
GP-LC-CNF-3	0.052	0.191	0.975	0.88	0.029	0.00
GP-LC-CNF-4	0.040	0.201	0.987	0.90	0.036	3.39
Hexyl Ester CNF	0.056	0.236	0.986	1.03	0.095	2.32
Phenyl Ester CNF	0.018	0.202	0.996	0.93	0.011	10.79
Na^+ Carboxyl CNF	0.018	0.043	0.997	0.85	0.016	2.42
Ethyl Cellulose	0.005	1.486	0.636	0.03	0.00	0.58
H^+ Carboxyl CNF	0.062	0.224	0.964	0.87	0.020	0.00
Hexyl Ether CNF	0.021	2.047	0.865	0.15	0.0031	0.73
Dodecyl Ether CNF	0.020	0.494	0.664	0.10	0.0012	0.00

* Parameters include root mean squared error (RMSE), normalized root mean square error (NRMSE), coefficient of determination (R^2), maximum normalized biogas production (V_{max}), biogas production rate (K), and lag phase (I).

Table S6. Assignment of ^{13}C-NMR chemical shifts (δ_{13C}) for untreated cellulose nanofibrils (CNF) and functionalized nanocellulose samples.*

	C=O	Aromatic C	C1	C4 (C)	C4 (A)	C2,3,5 (C)	C2,3,5 (A)	C6 (C)	C6 (A)	Aliphatic C
						δ_{13C} (ppm)				
CNF	n/a	n/a	105.4 102.5[†]	89.3	83.5 82.3[†]	73.0 72.0[†]	75.3 74.6[†]	65.5	63.0 61.5[†]	n/a
Phenyl Ester CNF	172.7 174.7[†]	134.5 129.5	105.3 101.9[†]	89.1	83.0 84.1[†]	72.6 71.9	75.2 74.6[†]	65.4	63.4 62.8[†]	41.3, 42.2[†]
Hexyl Ester CNF	176.0	n/a	104.7 97.7[†]	88.9	82.2 83.6[†]	72.9	75.1	65.2	62.5 60.0[†]	34.6, 31.7, 25.9, 22.9, 14.4
Na$^+$ Carboxyl CNF	175.7 177.6[†]	n/a	105.3	89.0 87.5[†]	83.8 81.4[†]	72.7 71.6[†]	74.9 74.5[†]	65.2	63.1 59.0[†]	n/a
Hexyl Ether CNF	n/a	n/a	104.2 100.5[†]	88.6	82.7	72.1	75.0	65.4	62.7	32.8, 31.0, 30.4, 27.5[†], 26.8, 23.6, 15.3
DA-CNF-2	181.9	n/a	105.2	89.0	83.7 81.4[†]	72.0	75.1	65.5	63.3 60.8[†]	35.5[†], 35.0, 33.1, 32.0[†], 30.5, 25.0, 23.4[†], 22.3[†], 16.5[†], 15.1
DA-CNF-3	181.6	n/a	105.2	88.7	83.1	72.0	74.7	65.2	62.4	34.7[†], 32.7, 30.0, 24.6, 14.7
DA-CNF-4	181.2	n/a	104.6 100.8[†]	88.6	83.4 82.0	71.2 72.1[†]	74.7 73.7[†]	64.6 65.3[†]	62.5 61.2[†] 59.6[†]	34.1, 33.2[†], 32.4, 31.3[†], 29.9, 25.4[†], 24.3, 22.7[†], 14.4, 12.2, 10.6
LC-CNF-1	181.0	n/a	104.4 101.2[†]	88.3	83.1 80.0[†]	71.7 71.2	74.3 73.6[†]	64.6 65.4[†]	62.1 61.3[†]	41.5, 34.2, 32.3, 31.4[†], 29.6, 24.2, 14.3
GP-LC-CNF-4	n/a	n/a	105.1 102.4[†]	89.0	83.6 82.4[†]	72.7 71.9[†]	75.1 74.5[†]	65.2 66.0[†]	62.7 60.9[†]	44.5, 43.7, 26.3[†], 23.2, 21.8, 20.5[†]

* Crystalline (C) and amorphous (A) forms are designated.

† Indicates a shoulder.

Table S7. Proportion of carbon 1-6 that is crystalline or amorphous in cellulose nanofibrils (CNFs) functionalized with the indicated ether, ester, and carboxyl groups.*

Sample	C-4		C-2,3,5		C-6		Average %C		Average %A	
	%C	%A	%C	%A	%C	%A	Avg	St Dev	Avg	St Dev
CNF	38	62	39	61	40	60	39	1.0	61	1.0
Phenyl Ester CNF	48	52	48	52	49	51	49	0.6	52	0.8
Hexyl Ester CNF	31	69	32	68	35	65	33	2.1	67	2.1
Na⁺ Carboxyl CNF	39	61	41	59	40	60	40	1.0	60	1.0
Hexyl Ether CNF	43	57	44	56	45	55	44	1.2	56	1.2
LC-CNF-1	51	49	50	50	51	49	51	1.0	49	1.0
DA-CNF-2	58	42	56	44	60	40	58	1.5	42	1.5
DA-CNF-3	56	44	55	45	57	43	56	1.1	44	1.1
DA-CNF-4	50	50	51	49	52	48	51	0.9	49	0.9
GP-LC-CNF-4	43	57	42	58	43	57	43	0.8	57	0.8

(Header spanning "^{13}C Crystallinity" over all columns except Sample)

* Crystalline (C), Amorphous (A), Cellulose Nanofibrils (CNF), Dodecanoic Acid (DA), and Gas Phase Lauroyl Chloride (GP-LC) are designated

Table S8. Computed $T_{1\rho H}$, T_{CH}, M_0, and DS values for carbon species in phenyl ester CNF and DA-CNF-2

Sample	Carbon Type	$T_{1\rho H}$ (µs)	T_{CH} (µs)	M_0	DS
Phenyl ester Cellulose	Aromatic	3700 ± 450	200 ± 140	4500 ± 160	0.087 ± 0.003
	Cellulose	6400 ± 150	180 ± 77	62400 ± 910	
DA-CNF-2	Methyl	18000 ± 1000	390 ± 21	1170 ± 8	0.192 ± 0.001
	Cellulose	9600 ± 380	247 ± 5	36600 ± 52	

Table S9. $DS_{surface}$ and $DS_{overall}$ values and Gompertz fit parameters for unmodified and functionalized cellulose nanofibrils.*

Sample	$DS_{surface}$	$DS_{overall}$	Normalized K	Normalized V_{max}
Unmodified Cellulose Nanofibrils				
Cellulose Nanofibrils	0	0	0.078	1.01
Liquid Phase Dodecanoic Acid Functionalization				
DA-CNF-1	0.014	0.035	0.037	0.95
DA-CNF-2 (Dodecyl Ester CNF)	0.097	0.45	0.020	0.94
DA-CNF-3	0.15	0.28	0.012	0.70
DA-CNF-4	0.43	0.20	0.009	0.67
Liquid Phase Lauroyl Chloride Functionalization				
LC-CNF-1	0.63	0.80	0.036	0.93
LC-CNF-2	0.67	0.82	0.031	0.71
LC-CNF-3	1.12	0.56	0.017	0.62
LC-CNF-4	2.46	1.16	0.019	0.37
Gas Phase Hexanoyl Chloride Functionalization				
GP-HC-CNF-1	1.19	0.17	0.031	1.01
GP-HC-CNF-2	1.54	0.16	0.023	0.90
GP-HC-CNF-3	1.89	0.14	0.013	0.66
GP-HC-CNF-4	2.43	0.14	0.013	0.70
Gas Phase Lauroyl Chloride Functionalization				
GP-LC-CNF-1	0.066	0.008	0.082	0.98
GP-LC-CNF-2	0.17	0.015	0.046	0.91
GP-LC-CNF-3	0.23	0.012	0.029	0.88
GP-LC-CNF-4	0.33	0.013	0.036	0.90

* Normalized rate (K) and maximum biogas production ($Vmax$) were obtained from Gompertz fits of normalized biogas production data. Cellulose Nanofibrils (CNF), Dodecanoic Acid (DA), Lauroyl Chloride (LC), Gas Phase Hexanoyl Chloride (GP-HC) and Gas Phase Lauroyl Chloride (GP-LC) are denoted.

Figures
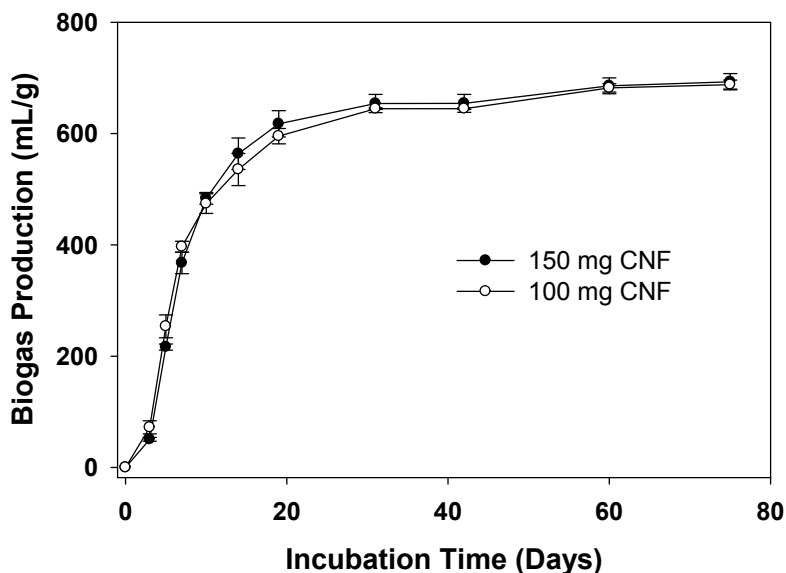
Figure S1. Biogas production during mineralization of 150 mg (black circles) and 100 mg (white circles) cellulose nanofibrils (CNF) by an anaerobic microbial community. Biogas production was normalized for mass loading. Error bars represent one standard deviation from triplicate samples.
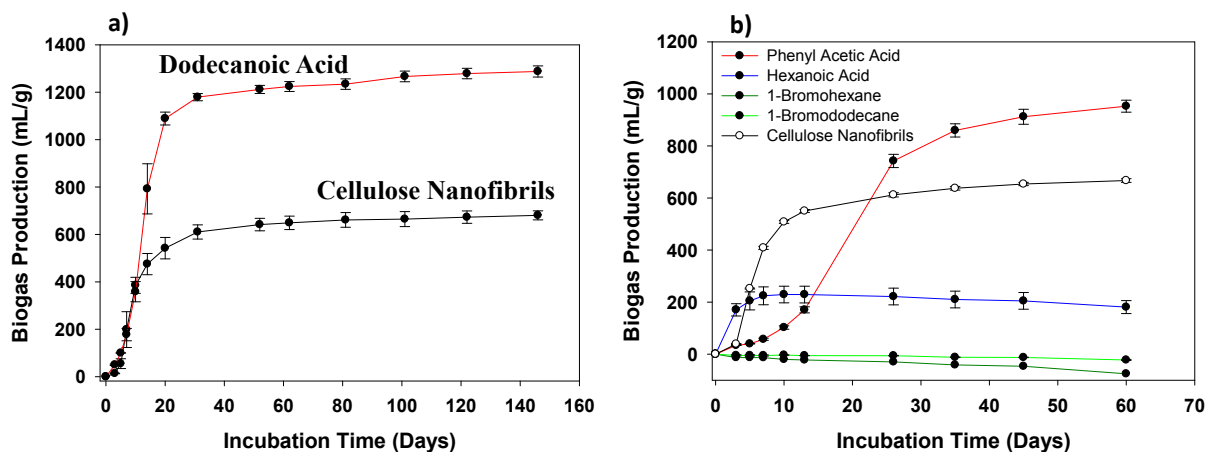
Figure S2. a) Biogas production during mineralization of dodecanoic acid and cellulose nanofibrils by an anaerobic microbial community. b) Biogas production during mineralization of functionalization reagents. In both panels, error bars represent one standard deviation from the average of duplicate samples.
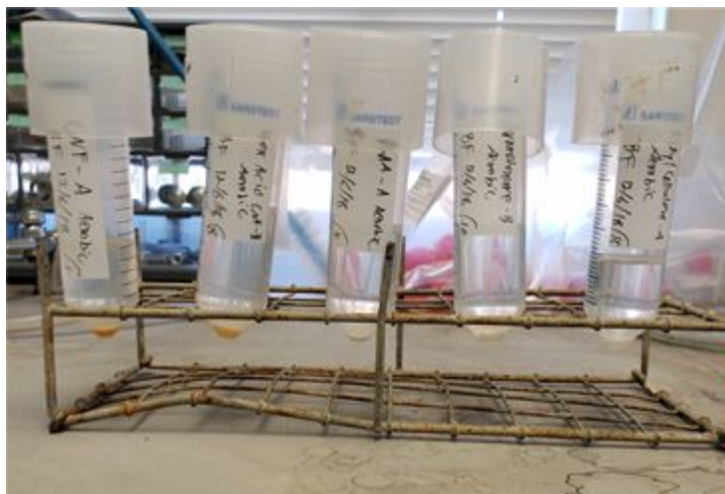
Figure S3. Digital images of functionalized cellulose nanofibrils after 60 d of exposure to an aerobic microbial community in 50 mL conical vials.
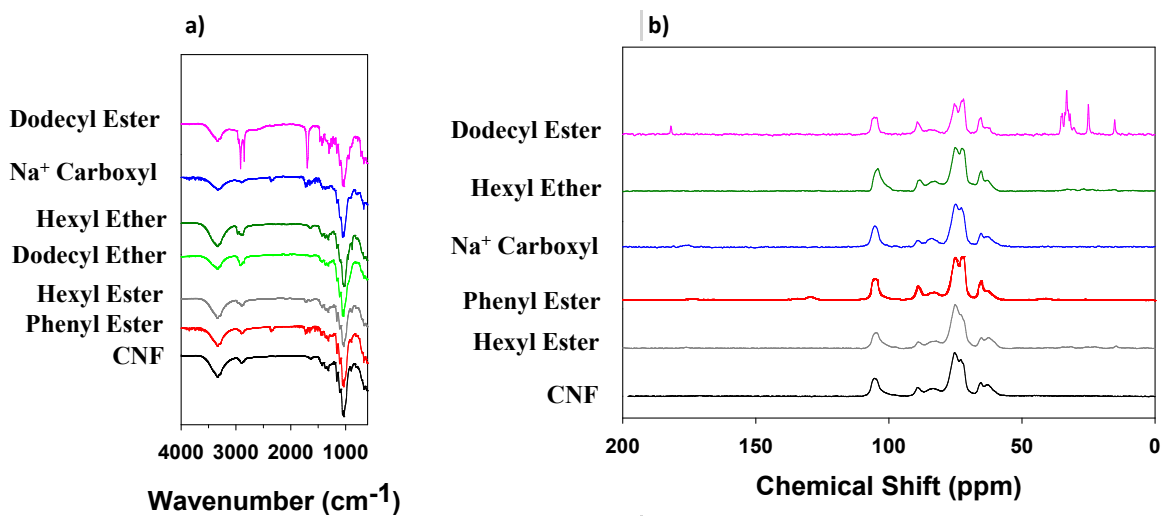
Figure S4. a) Infrared and b) ^{13}C-NMR spectra of cellulose nanofibrils (black) functionalized with dodecyl (pink), hexyl (grey), and phenyl (red) esters as well as hexyl (dark green) and dodecyl (light green) ethers and carboxylic acid (blue).
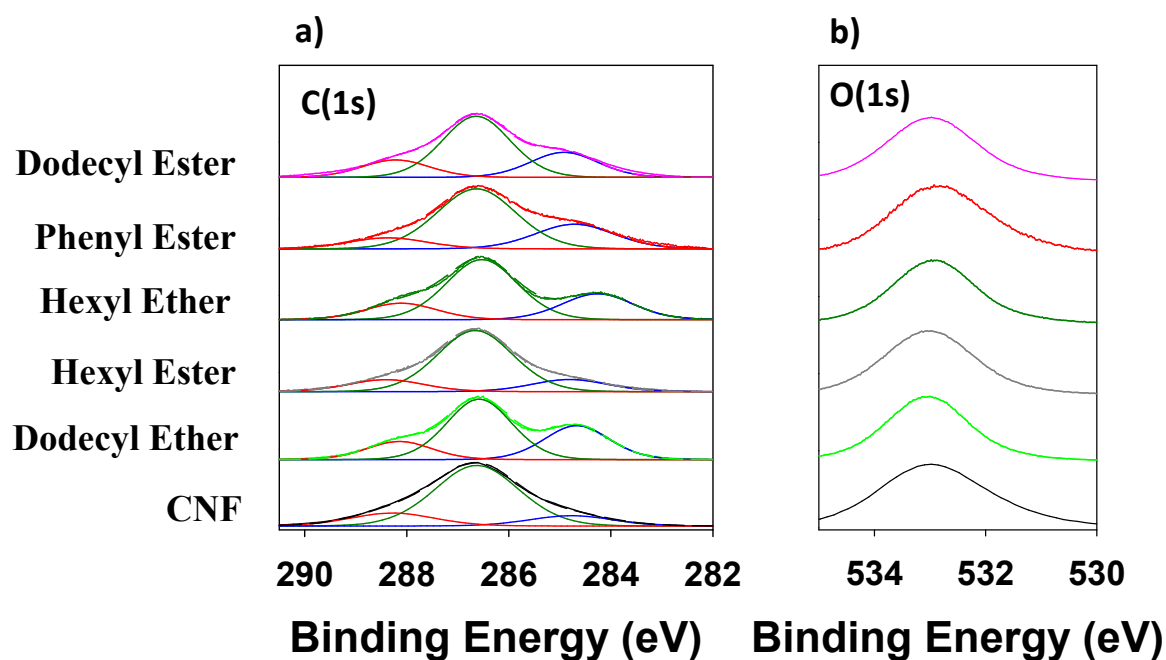
Figure S5. X-ray photoelectron spectra. a) C(1s) with component peak fitting and b) O(1s) regions of cellulose nanofibrils (CNFs) and CNFs functionalized with dodecyl (pink), phenyl (red), and hexyl (grey) esters and dodecyl (light green) and hexyl (dark green) ethers.
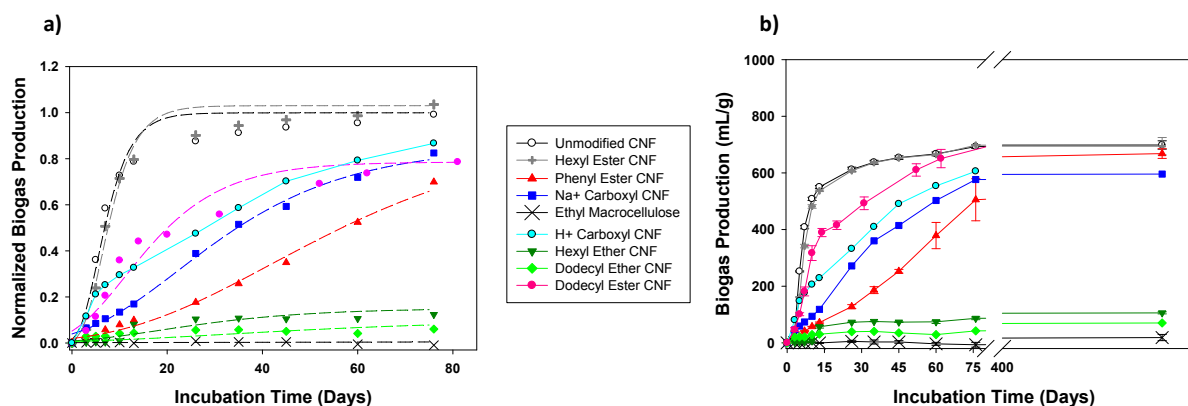
Figure S6. a) Normalized (dotted lines are fits from Gompertz model) and b) unnormalized biogas production (not fitted, as denoted by solid lines) from the mineralization of cellulose nanofibrils (CNF) and CNFs functionalized with hexyl ester, dodecyl ester, carboxylic acid with Na^+ and H^+ counterions, phenyl ester, hexyl ether, and dodecyl ether as well as commercial ethyl macrocellulose. Error bars represent one standard deviation of duplicate samples.
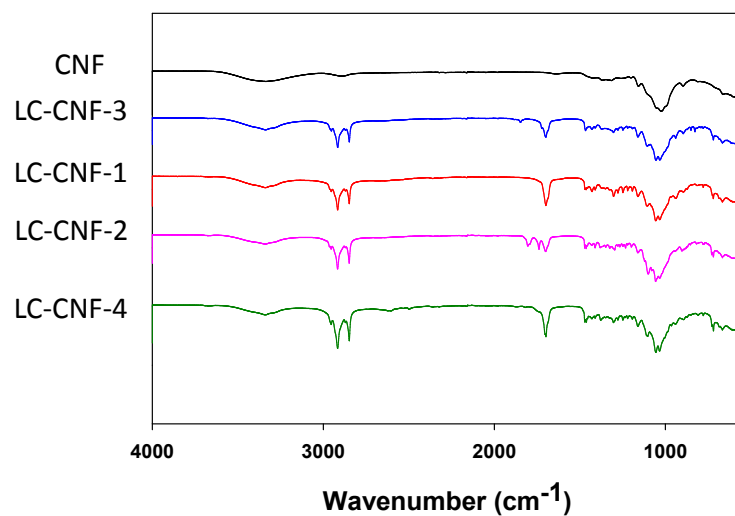
Figure S7. Infrared spectra of cellulose nanofibrils (CNF) esterified with lauroyl chloride (LC-CNF).
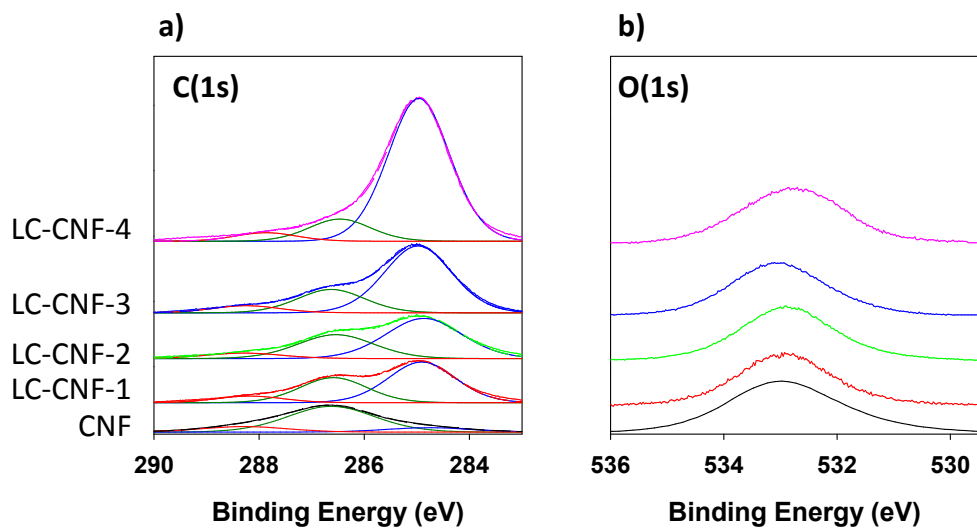
Figure S8. X-ray photoelectron spectra. a) Fitted C(1s) and b) O(1s) regions of cellulose nanofibrils (CNF) esterified with lauroyl chloride (LC-CNF).
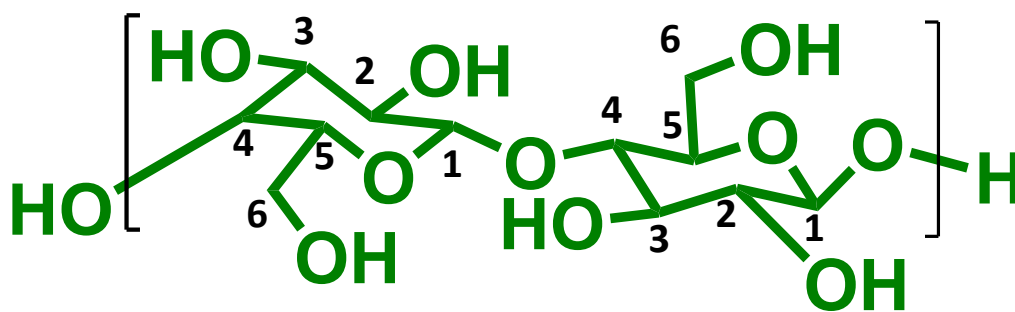
Figure S9. Nanocellulose repeat unit (cellobiose) with carbons 1-6 labeled for each glucose subunit.
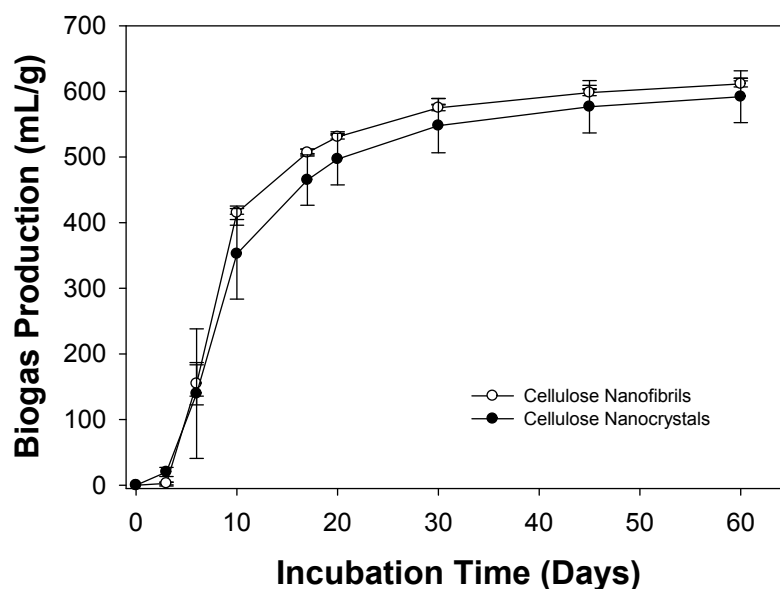

Figure S10. Biogas production of cellulose nanofibrils (CNFs) compared to cellulose nanocrystals (CNCs). Data is not fit to the Gompertz model as denoted by the solid connecting lines. Error bars represent one standard deviation from triplicate samples.
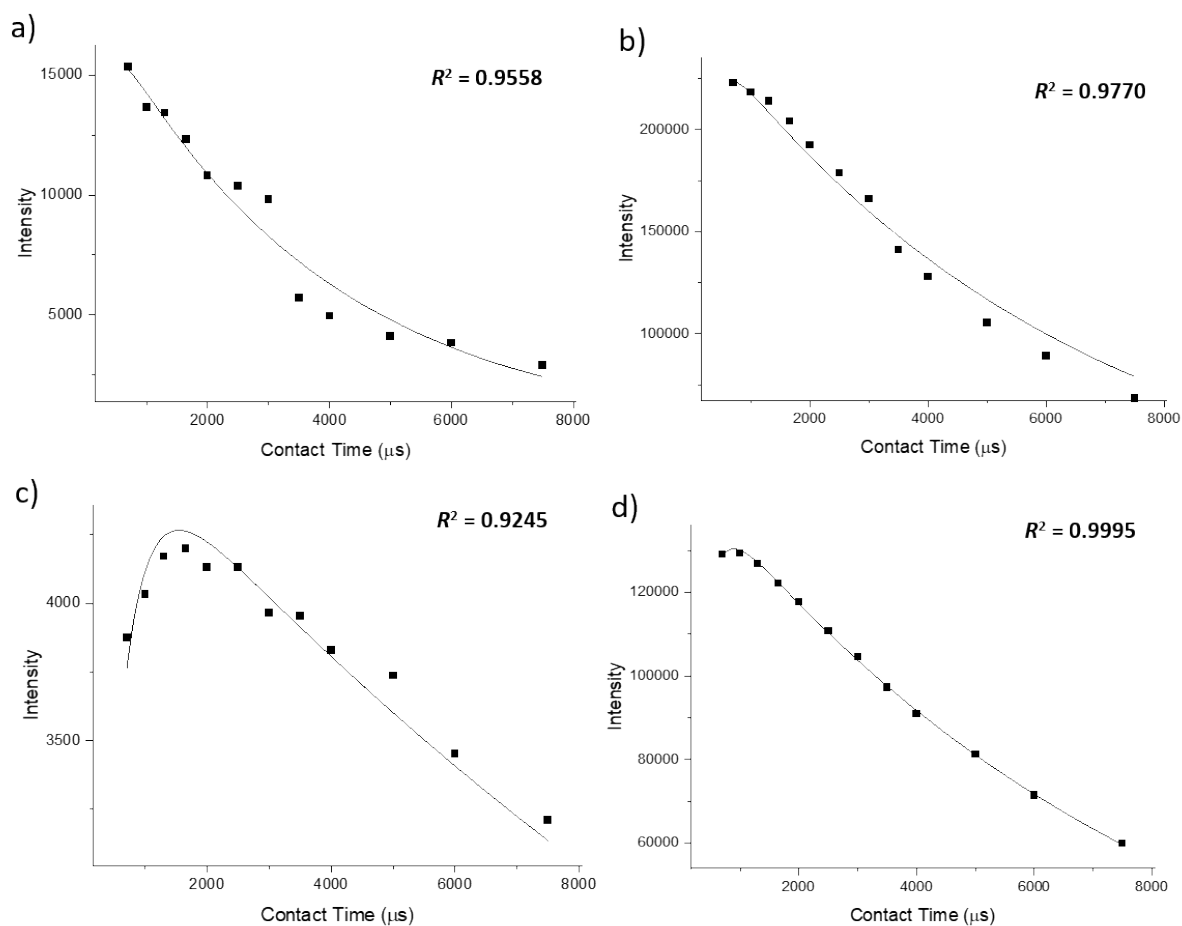
Figure S11. Signal intensity as a function of contact time for a) phenyl ester CNF aromatic carbons, b) phenyl ester CNF cellulose carbons, c) DA-CNF-2 methyl carbons, and d) DA-CNF-2 cellulose carbons from variable contact time CP-MAS experiments. Symbols represent experimental data. Lines correspond to least squares fit according to equation S1 with R^2 values displayed.
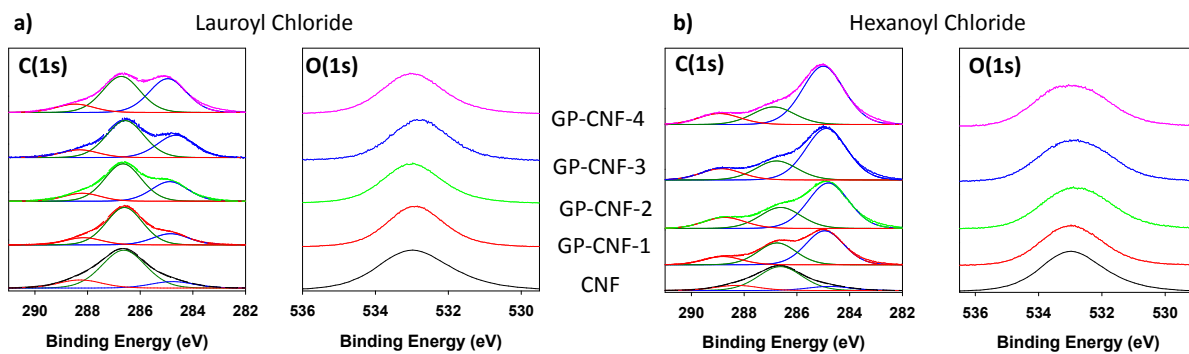
Figure S12. Fits of X-ray photoelectron spectra for the C(1s) and O(1s) regions for cellulose nanofibrils (CNFs) functionalized with gas phase (GP-CNF) a) lauroyl chloride and b) hexanoyl chloride.
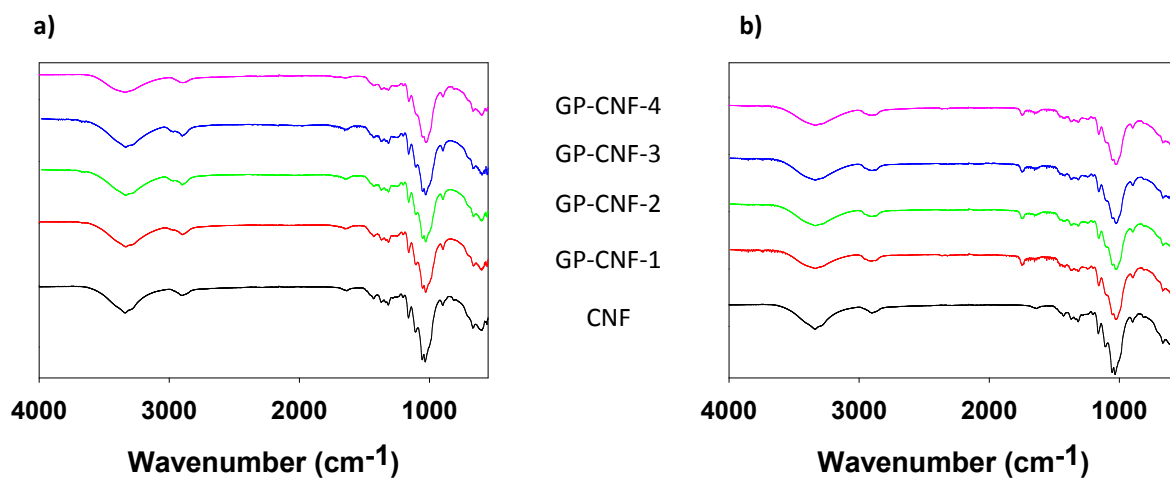

Figure S13. Infrared spectra of cellulose nanofibrils (CNF) esterified with gas phase (GP) a) lauroyl chloride (LC-CNF) and b) hexanoyl chloride (HC-CNF).
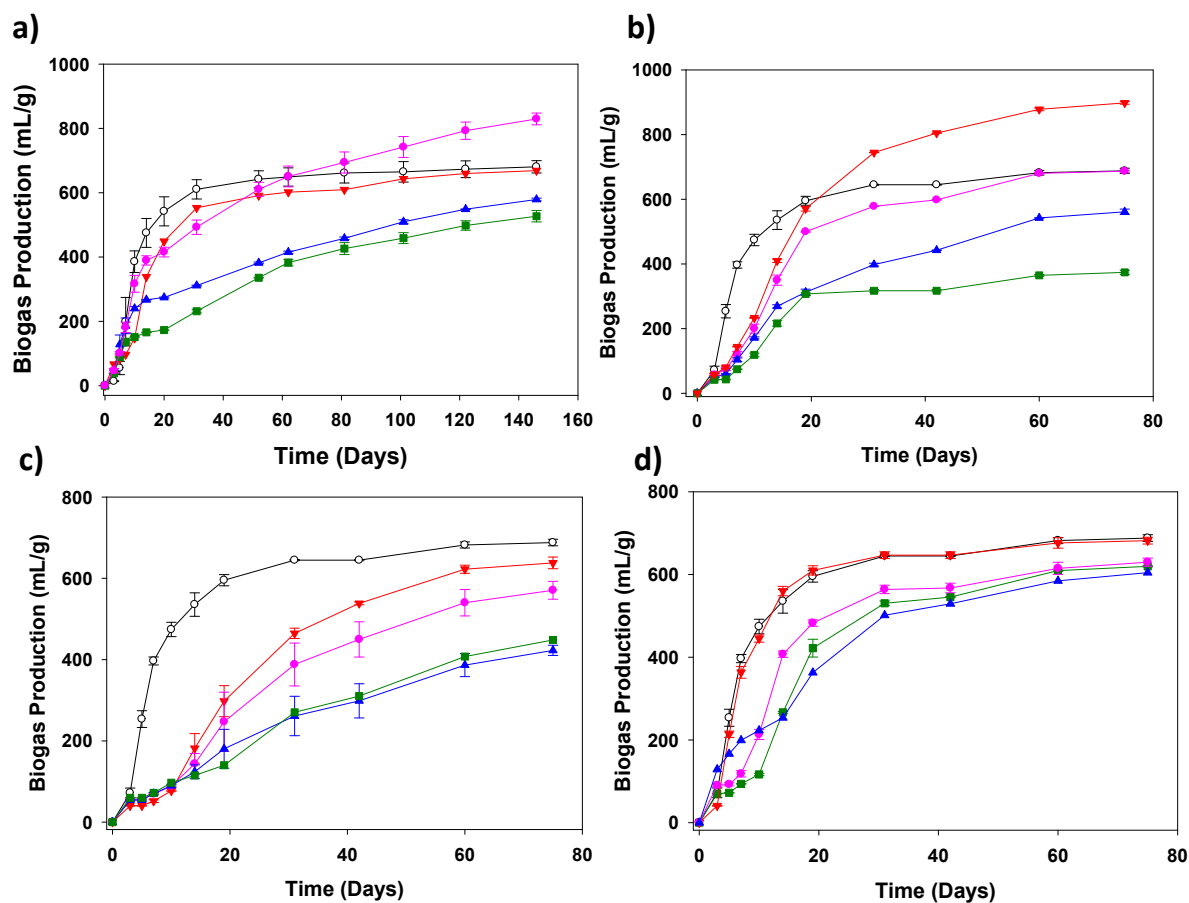
Figure S14. Unnormalized biogas production of cellulose nanofibrils functionalized with a) liquid-phase dodecanoic acid, b) liquid-phase lauroyl chloride, c) gas-phase hexanoyl chloride, and d) gas-phase lauroyl chloride during mineralization by an anaerobic microbial community. In each sample set, the number corresponding to degree of surface substitution increases from 1-4 as: red, pink, blue, green. In each plot, error bars represent one standard deviation of the average from duplicate samples.
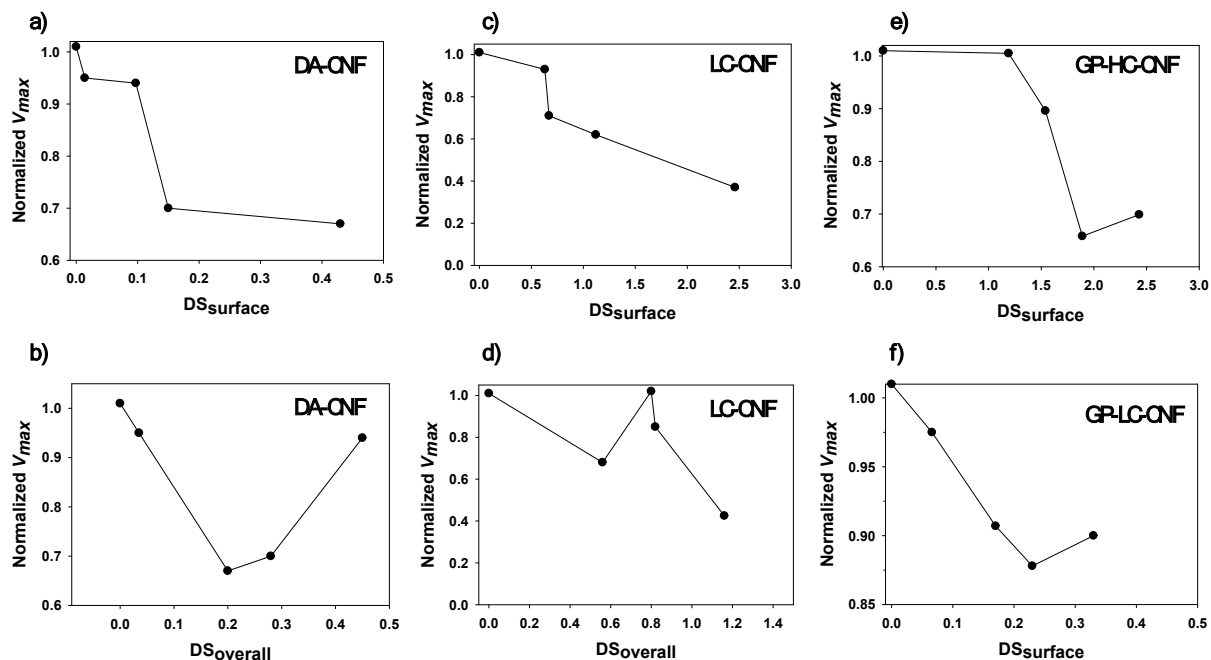
Figure S15. Relation of $DS_{surface}$ and $DS_{overall}$ with normalized maximum biogas production (V_{max}) for CNF esters functionalized with (a,b) dodecanoic acid (DA) and (c,d) lauroyl chloride (LC). Also shown is the correlation of $DS_{surface}$ with normalized maximum biogas production for CNF esters functionalized with (e) gas phase (GP) hexanoyl chloride (HC) and (f) gas phase lauroyl chloride.

REFERENCES

1.   Frank, B. P.; Durkin, D. P.; Caudill, E. R.; Zhu, L.; White, D. H.; Curry, M. L.; Pedersen, J. A.; Fairbrother, D. H., Impact of Silanization on the Structure, Dispersion Properties, and Biodegradability of Nanocellulose as a Nanocomposite Filler. *ACS Applied Nano Materials* **2018,** *1* (12), 7025-7038.
2.   Loof, D.; Hiller, M.; Oschkinat, H.; Koschek, K., Quantitative and Qualitative Analysis of Surface Modified Cellulose Utilizing TGA-MS. *Materials* **2016,** *9* (6), 415.
3.   Kinchesh, P.; Powlson, D. S.; Randall, E. W., C-13 Nmr-Studies of Organic-Matter in Whole Soils .1. Quantitation Possibilities. *Eur J Soil Sci* **1995,** *46* (1), 125-137.
4.   Dai, X.; Chen, Y.; Zhang, D.; Yi, J., High-solid Anaerobic Co-digestion of Sewage Sludge and Cattle Manure: The Effects of Volatile Solid Ratio and pH. *Sci. Rep.* **2016,** *6* (1), 35194.
5.   Mei, R.; Narihiro, T.; Nobu, M. K.; Kuroda, K.; Liu, W.-T., Evaluating digestion efficiency in full-scale anaerobic digesters by identifying active microbial populations through the lens of microbial activity. *Sci. Rep.* **2016,** *6* (1), 34090.
6.   Yi, J.; Dong, B.; Jin, J.; Dai, X., Effect of increasing total solids contents on anaerobic digestion of food waste under mesophilic conditions: performance and microbial characteristics analysis. *PloS one* **2014,** *9* (7), e102548-e102548.
7.   Baptista, M. Modelling of the kinetics of municipal solid waste composting in full-scale mechanical biological treatment plants. New University of Lisbon, 2009.